Spatial-Temporal Hidden Markov Model for Land Cover Classification Using Multitemporal Satellite Images

CHUNLIN LIU[1,4]**, WEI SONG**[2]**, CHUNXIA LU**[3]**, AND JIANXIN XIA**[1,4]

[1]College of Life and Environmental Science, Minzu University of China, Beijing 100081, China
[2]School of Information Engineering, Minzu University of China, Beijing 100081, China
[3]Institute of Geographic Sciences and Natural Resources Research, Chinese Academy of Sciences (CAS), Beijing 100101, China
[4]Key Laboratory of Ecology and Environment in Minority Areas, National Ethnic Affairs Commission, Minzu University of China, Beijing 100081, China

Corresponding author: Jianxin Xia (jxxia@vip.sina.com)

ABSTRACT Land cover is of great significance for the study of global ecological environmental change. Multitemporal land cover can help us to understand the change process of the regional environment and formulate corresponding protection policies. For single-period image classification, the spatial-temporal information is often ignored, and the classification accuracy is difficult to improve. In this paper, an iterative hidden Markov model (STHMM) is proposed to optimize the multitemporal classification, in which a stacked autoencoding classifier is used to calculate the initial class probability, and the extended random walker-based spatial optimization technique is adopted to optimize the class probability. Finally, the hidden Markov model with expectation maximization is built by exploiting postprocessing temporal optimization. Experimental results show that the proposed method can outperform other classification techniques, and the spatial-temporal hidden Markov model proposed in this paper exhibits more stable and reliable performance and can be widely used in multitemporal classification.

INDEX TERMS Hidden Markov model, land cover classification, multitemporal satellite images, spatial-temporal information.

I. INTRODUCTION

Land cover is a sensitive indicator of eco-environmental change, which plays an essential role in global climate change [1]–[3]. With the development of the social economy and the continuous intensification of industrial activities, air pollution and soil erosion have become more serious. Multitemporal classification is the basis for the study of the global ecological environment, and the purpose is to better understand the change in land cover. Therefore, it is of considerable significance to study the multitemporal land cover classification method and analyze the law of land cover change to improve the protection and restoration of the global environment and promote the construction of an ecological civilization [4]–[7].

The traditional manual collection of land cover information requires high cost and labor, and it is difficult to obtain

The associate editor coordinating the review of this manuscript and approving it for publication was Stefania Bonafoni.

large-scale and multiperiod land cover distribution information. With the continuous development of remote sensing technology, satellite remote sensing technology has the advantages of extensive area monitoring, short cycles, and low cost and has been widely used in land cover classification [8]–[13]. At present, when remote sensing images are used for large-scale land cover classification, the classification accuracy cannot be significantly improved [14], [15]. The reason for this is that most of the existing classification technologies only focus on single temporal images and do not make full use of the temporal information of multitemporal images, so the improvement of classification accuracy is limited. Therefore, the multitemporal classification method will be an important research direction of the new classification strategy [16]–[20]. There are two kinds of land cover classification methods considering temporal context information. The first method is to make a standard land cover classification map, and then the classification map is updated dynamically by spectral change information. This method is
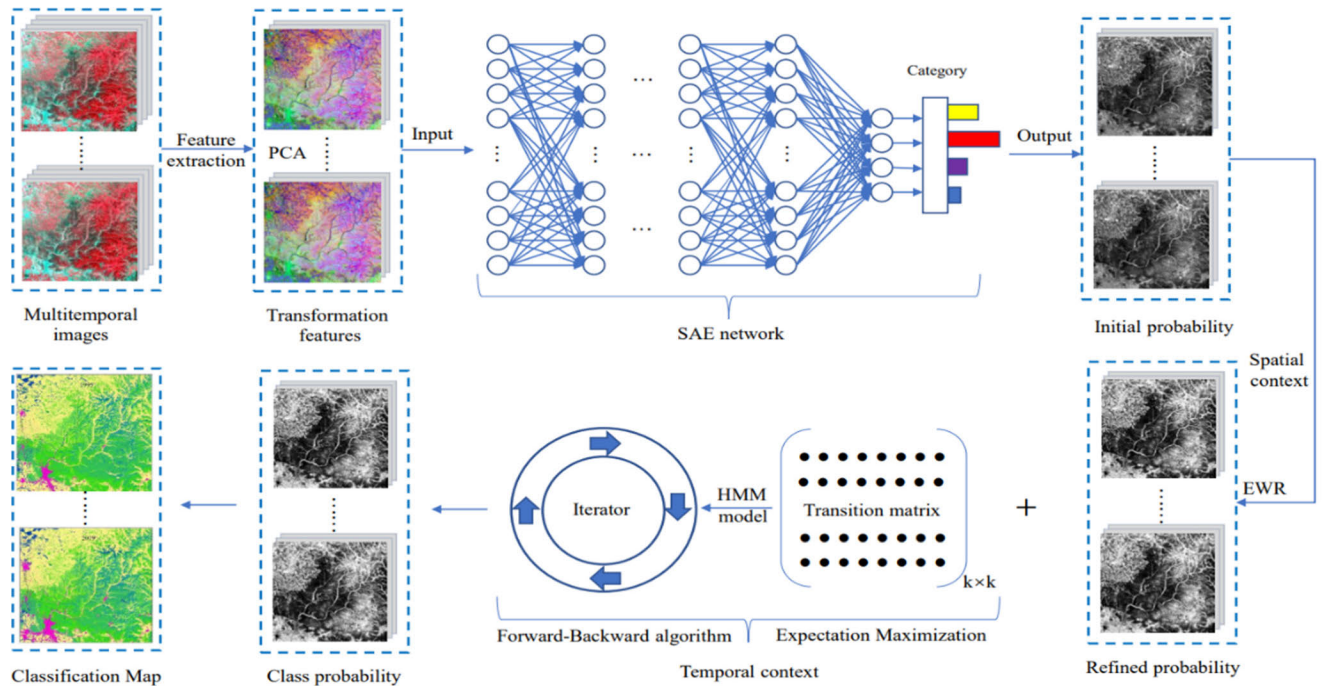
IEEE *Access*

C. Liu *et al.*: Spatial-Temporal Hidden Markov Model for Land Cover Classification Using Multitemporal Satellite Images

FIGURE 1. Flow chart of the proposed classification method.

simple and more conducive to multitemporal land cover classification [21]; its premise is that the change in spectral information can truly reflect the change in different land types. However, the imaging conditions and processing methods in different periods will have adverse effects [22]. Another method is to add multiperiod land cover change information to classification and independently produce the land cover products of each period [23]. For example, Friedl *et al.* [24] applied a multitemporal enhanced vegetation index to produce global land cover products and used spatial information to optimize the classification results. In [25], a spatial MRF framework was extended by a temporal energy term based on a transition probability matrix. In [26], the maximum a posterior probabilistic Markov random field model (MAP-MRF) was proposed, and some researchers improved MAP-MRF by using spatial-temporal context information [27]. In [28], conditional random fields (CRFs) were expanded by temporal interaction terms that link neighboring epochs via transition probabilities between different classes. In addition, Abercrombie *et al.* [29] proposed a method that used a hidden Markov model to help distinguish real land cover change from spurious land cover changes in classification time series, and a hidden Markov model (HMM) as used as postprocessing to optimize the initial classification results. However, in the study of land cover classification based on time series, it is difficult to consider temporal correlation and spatial continuity. Although some methods consider the temporal and spatial relationship at the same time, too many parameters make the model difficult to widely use, the transfer matrix is obtained by experience setting, and the flexibility is limited.

To solve these problems, this paper proposed an iterative HMM to optimize the multitemporal classification, in which a stacked autoencoding (SAE) classifier is used to calculate the initial class probability, and the extended random walker (ERW)-based spatial optimization technique is adopted to optimize the class probability. Lan M *et al.* [30] proposed using three remaining expansion blocks to construct an expanded convolutional neural network encoder, which can effectively extract roads. The ERW is considered to model the spatial information between neighboring pixels. Finally, an HMM with expectation maximization (EM) is built by exploiting postprocessing temporal optimization, and the EM is used to solve the transfer matrix to obtain more realistic land cover change. Fig. 1 presents the flow chart of the proposed method, which is comprised of three key steps: initial classification probability, spatial optimization, and temporal optimization. The detailed steps are shown below.

II. MATERIALS AND METHODS
A. OVERVIEW OF THE RESEARCH AREA
We chose the Chongli District as the study area (Fig 2). The area is located between 40°47'-41°17' N and 114°17'-115°34' E, the area is rich in natural resources, and it is one of the counties with the largest natural forest area in Hebei Province. According to the actual situation of the study area, we followed the classification standard of the International Geosphere-Biosphere Programme (IGBP). The study area is divided into seven types: cropland (CL), built-up lands (BL), needleleaf forests (NF), broadleaf forests (BF), shrublands (SL), grasslands (GL) and water bodies (WB). Through a field survey in 2019, 37 points were selected in the study
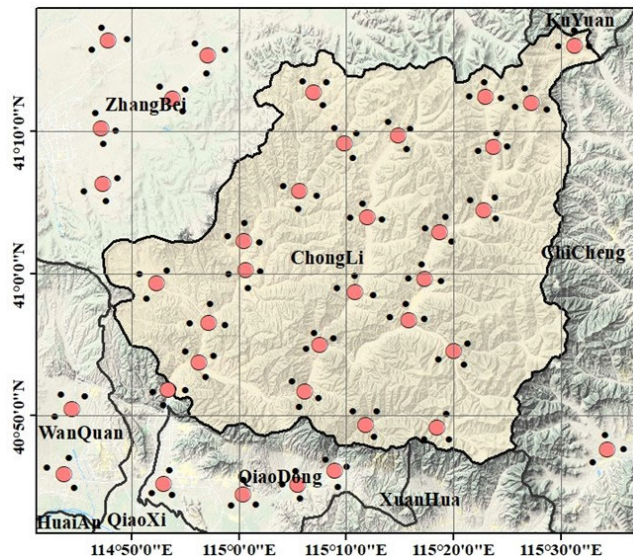
C. Liu *et al.*: Spatial-Temporal Hidden Markov Model for Land Cover Classification Using Multitemporal Satellite Images

IEEE *Access*

FIGURE 2. The study area and distributions of survey stations.

area. Each measuring point contained three sub measuring points, and a polygon of the sample label was drawn in each sub measuring point contained about 200 pixels on average, the total number of pixels in the image is 22,000. The uniform distribution of measuring points in the study area recorded the latitude and longitude coordinates. We used two-thirds of the data for training, and the remaining data were used for accuracy verification.

B. DATA SELECTION AND PROCESSING
The data used in the study are landsat5 and landsat8. The revisit period of the data is 16 days, and its spatial resolution is 30 m. Radiometric calibration and atmospheric correction have been performed before using the data. Due to the complexity and diversity of land cover types in the study area, different features may have similar spectral characteristics, and the same features may also have different spectral characteristics. A single period of remote sensing images is not conducive to land cover classification. In this paper, we chose the data from 1995 to 2019 to include as many seasons as possible, the images of multiple periods in a year are combined, and then principal component analysis is performed, which is conducive to more accurate classification. Figure 3 shows the display result of standard false color.

C. HMM MODEL
The hidden Markov model (HMM) is a probabilistic model of a timing sequence that describes the process of generating a nonobservable state random sequence from a hidden Markov chain and then generating an observed random sequence from various states [33]. The initial probability distribution mainly determines it, transition probability and observation probability distribution. The form of HMM is defined as follows: Q is a set of all possible states, V is all the observation set $V = \{v_1, v_2, \cdots, v_M\}$, and M is the number of possible
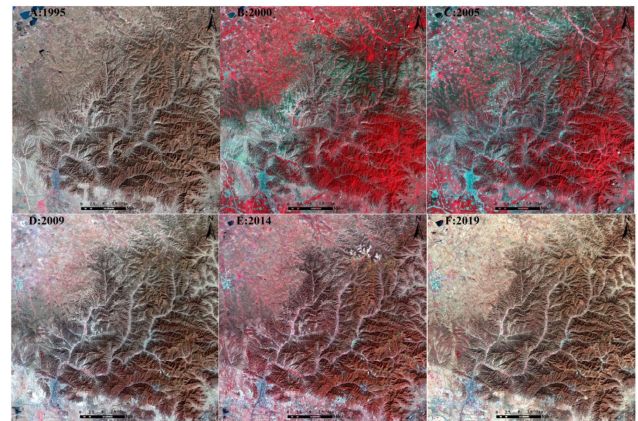

FIGURE 3. Remote sensing distribution map of the study area.

observations. I is the sequence of the length T state $I = \{i_1, i_{2,\cdots}, i_T\}$, and O corresponds to the sequence of observations $O = \{o_1, o_2, \cdots, o_T\}$. A is the state transition matrix $A = [a_{ij}]_{N \times N}$, where $a_{ij} = P(i_{t+1} = q_j | i_t = q_i)$, indicating the probability of transition to state q_j at time t+1 under the condition of q_i at time t, where $b_{ik} = P(o_t = v_k | i_t = q_i)$, b_{ik} is the probability of producing the observed v_k under the condition of q_i at time t. $\pi_i = P(i_1 = q_i)$, the probability of q_i at t = 1.

In general, HMM applications include two prerequisites. First, the state at any moment is only dependent on the state at the previous moment and has nothing to do with the state at other moments. Second, the observed value at any time depends only on the state at that time and is independent of the state at other times. In a given model $\lambda = (A, B, \pi)$ and the observation sequence $O = \{o_1, o_2, \cdots, o_T\}$, the probability of occurrence of the observation sequence is $P(O|\lambda)$. The probability calculation problem in an HMM can be solved by a forward-backward algorithm.

The probability that the partial observation sequence is $o_1, o_2, \cdots, o_t$ and the state is q_i at the moment is called the forward probability, which is expressed as:

$$\alpha_t(i) = P(o_1, o_2, \cdots, o_t, i_t = q_i | \lambda) \qquad (1)$$

Initial value: $\alpha_1(i) = \pi_i b_{io_1}$, when t = 1, 2, $\cdots$, T − 1, then

$$\alpha_{t+1}(i) = \left(\sum_{j=1}^{N} \alpha_t(j)a_{ji}\right) b_{io_{t+1}} \qquad (2)$$

Probability of observation sequence:

$$P(O|\lambda) = \sum_{i=1}^{N} \alpha_T(i) \qquad (3)$$

Backward algorithm: For a given backward algorithm λ, on the premise that the state at moment t is defined q_i, the partial observation sequence from to is $o_{t+1}, o_{t+2}, \cdots, o_T$ and the probability is called the backward probability, which

is expressed as:

$$\beta_t(i) = P(o_{t+1}, o_{t+2}, \cdots, o_T \mid i_t = q_i, \lambda) \qquad (4)$$

Initial value $\beta_T(i) = 1$, when $t = T - 1, T - 2, \cdots, 1$, then

$$\beta_t(i) = \sum_{j=1}^{N} \left(a_{ij} b_{jo_{t+1}} \beta_{t+1}(j)\right) \qquad (5)$$

The observation sequence can finally be expressed as:

$$P(O|\lambda) = \sum_{i=1}^{N} \pi_i b_{io_1} \beta_1(i) \qquad (6)$$

According to the definition of the forward and backward algorithm, we know:

$$P(i_t = q_i, O|\lambda) = \alpha_t(i) \beta_t(i) \qquad (7)$$

Therefore, given a model λ and observation sequence O, the probability of being in a state q_i at moment t can be expressed as:

$$P_t(i_t = q_i|O, \lambda) = \frac{\alpha_t(i)\beta_t(i)}{\sum_{i=1}^{N} \alpha_t(i)\beta_t(i)} \qquad (8)$$

D. SPATIAL-TEMPORAL HMM
1) SPATIAL OPTIMIZATION
It is easy to produce some small objects during the classification process. To alleviate this problem, a postprocessing spatial probability optimization method is proposed, which is an effective supplementary method that can avoid the excessive smoothing caused by feature extraction. ERW is used to optimize the initial probability [31]. Specifically, the classification probability can be optimized by the following formula:

$$E(i_t|O) = E_s(i_t|O) + \gamma E_{as}(i_t|O) \qquad (9)$$

where E_s is the spatial term, E_{as} is the aspatial term, and γ is the equilibrium parameter. The spatial term can be calculated by adjacent pixels:

$$E_s(i_t|O) = P(i_t|O)^T L P(i_t|O) \qquad (10)$$

where L is the normalized Laplacian matrix. The second term can be expressed as the integral of the initial probability:

$$E_{as}(i_t|O) = \sum_{j_t=1, j_t \neq i_t} P(j_t|O)^T \wedge_{j_t} P(j_t|O)$$
$$+ (P(i_t|O) - 1)^T \wedge_{i_t} (P(i_t|O) - 1) \qquad (11)$$

where $\wedge$ is the diagonal matrix, and the diagonal value is composed of the initial probability. Finally, the refined probability $P(i_t|O)$ is obtained by optimizing Eq (12). The weighted fusion is considered to merge the class probabilities of the two stages:

$$P(i_t|O) = (1 - \mu)P_s(i_t) + \mu P_t(i_t|O) \qquad (12)$$

where μ is a super parameter used to adjust the weight balance spatial-temporal stability. Finally, the state of the maximum posterior probability is solved.

2) PARAMETER ESTIMATION
(1) The initial probability: the initial probability represents the probability that the pixel belongs to each category in the initial year. The SAE classifier is used to calculate the probability of land cover classification in each year, in which SoftMax cross entropy is used to construct the loss function, which satisfies the constraint that the sum of probability of each category is 1. In this paper, the initial probability is calculated by the average probability of each year.

(2) The transition matrix: The transition matrix represents the transition probability between different land cover types in two adjacent years. In [29], the author analyzed the change law of global map coverage and found that the 90% probability of surface coverage type did not change. However, the parameters of the transfer matrix need to be set artificially, and the method is inflexible. Therefore, this paper uses the expectation maximization (EM) algorithm to calculate the transfer matrix. In [32], the author proves the effectiveness of the method:

$$P(i_{t+1}|j_t)$$
$$= P(i_{t+1}, j_t)/P(j_t) \qquad (13)$$
$$P_{i_{t+1}}(i_{t+1}, j_t)$$
$$= \frac{1}{S \cdot P(i_{t+1}) P(j_t)} \cdot$$
$$\sum_{n=1}^{N} \frac{P_{it}(i_{t+1}^n, j_t^n) P(i_{t+1}^n|O_n) P(j_t^n|O_n)}{\sum_{k \in \Omega} \sum_{h \in \Omega} \frac{P(k_{t+1}^n, h_t^n)}{P(k_{t+1}^n) P(h_t^n)} P(k_{t+1}^n|O_n) P(h_{t_t}^n|O_n)}$$
$$\qquad (14)$$

where i_t is the current iteration, S is the number of pixels, N is the number of classes, and Ω is the set of all labels.

To consider the correlation between neighboring pixels and remove small objects, the EWR algorithm is used to optimize the initial probability. In each calculation, the new transition matrix and spatial probability are recalculated, and the three elements of the hidden Markov model are input into the forward backward algorithm to update the classification probability dynamically. Finally, we output labels by maximizing the posterior probability.

III. RESULTS
A. EQUATIONSTIME SERIES CLASSIFICATION
In this paper, we compare three methods: the first is the SAE without postprocessing. The hidden layer is 3 layers, the number of nodes in each layer is 200, the learning rate is 3e-4, and the regularization parameter is 1e-6.the other is the classification result processed by the hidden Markov model, and the last is the result processed by the method proposed in this paper. The classification results are shown in Fig 4. The accuracy of the results after the STHMM method is improved. We also found that over the years, construction land has gradually increased, but the cultivated land area has exhibited
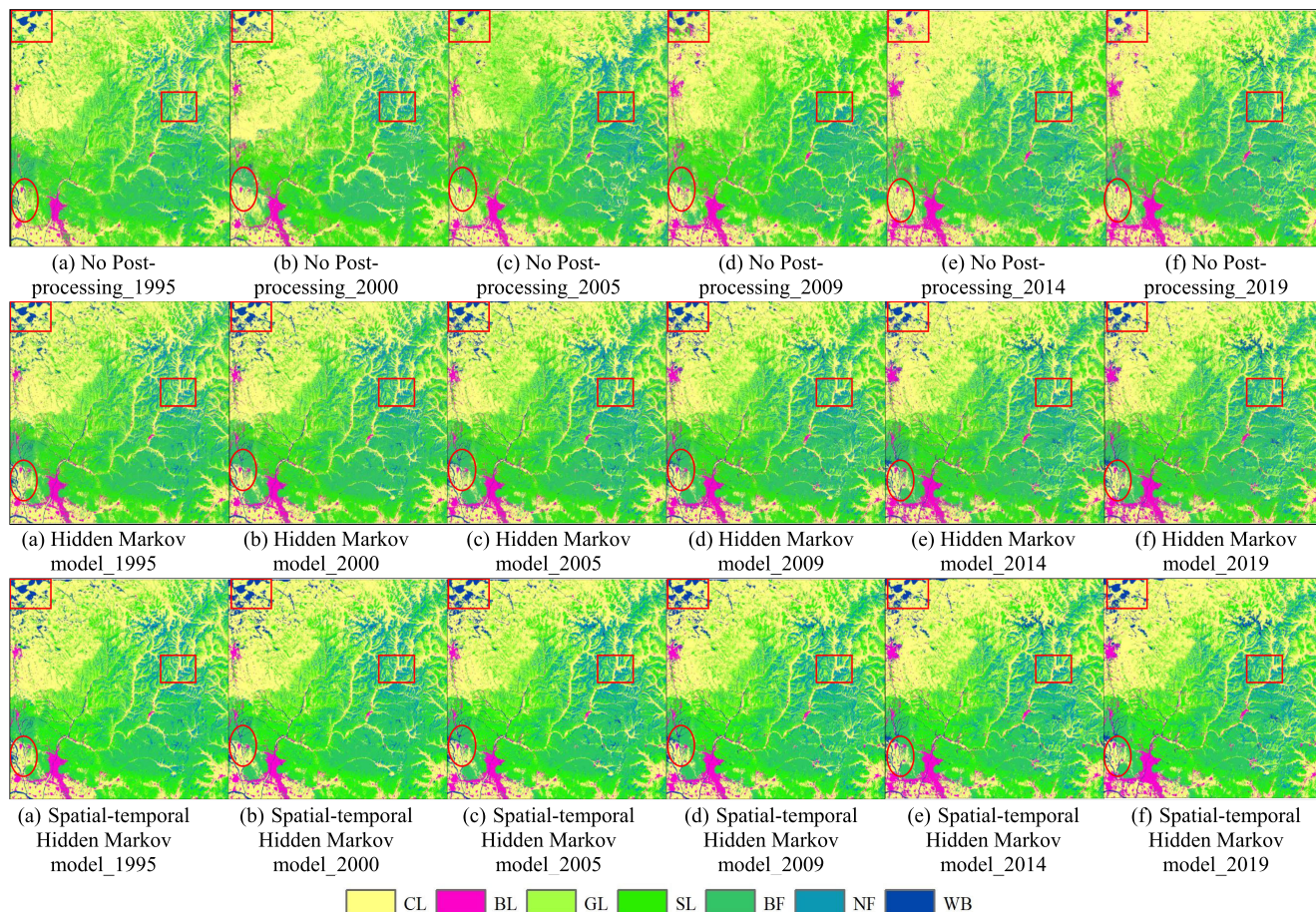
C. Liu *et al.*: Spatial-Temporal Hidden Markov Model for Land Cover Classification Using Multitemporal Satellite Images

IEEE *Access*

| CL | BL | GL | SL | BF | NF | WB |

FIGURE 4. Vegetation classification results in each period from 1995 to 2019: (a) indicates the classification results of the original classifier, (b) indicates the classification results after HMM processing, and (c) indicates the spatial and temporal HMM classification result.

almost no change, mainly because the ecological environment has been significantly changed by human beings, which leads to the expansion of urban areas. In Fig 5, the classification results with NPP are not continuous in temporal distribution. For the HMM, each type shows a stable correlation in the time series, but some classification results show small objects in the spatial distribution, which shows the best advantage with the STHMM considering the spatial-temporal relationship, and the temporal and spatial distributions are reasonable. In the initial classification results, Fig 5 contains some illogical transformations among cultivated land, construction land, water bodies, and forests, while the updated map dramatically improves the results. Due to the influence of image quality, environmental change, classifier performance and other factors, there are some unreliable patches in the multitemporal classification image, such as the classification results changing frequently after a period of time. This phenomenon is obviously improved after considering the temporal and spatial neighborhood relations.

B. PRECISION INSPECTION AND EVALUATION
The quality evaluation of multitemporal classification is necessary to describe the reliability of classification results.

However, traditional evaluation methods often verify the accuracy by selecting some measured sample data. They cannot fully reflect the spatial and temporal correlation of coverage types. Therefore, this kind of evaluation method is not sufficiently representative. To fully evaluate the pros and cons of this method, this paper evaluates the classification results from two aspects. First, the overall classification accuracy of the measured data test results, and second, a joint probability index is proposed to reflect the time and space between categories.

1) ACCURACY EVALUATION
To evaluate the classification accuracy and stability of STHMM, two-thirds of the samples are used for training, and the remaining one-third of the samples are used for accuracy verification. These test samples are evenly distributed throughout the study area. It can better represent the surface coverage of the entire study area. We select two commonly used evaluation indexes, the overall accuracy and kappa coefficient, and the statistical results are shown in the table.

Table 2 shows the overall classification accuracy and Kappa coefficient of the three methods in different periods. The overall classification accuracy (overall accuracy, OA) is
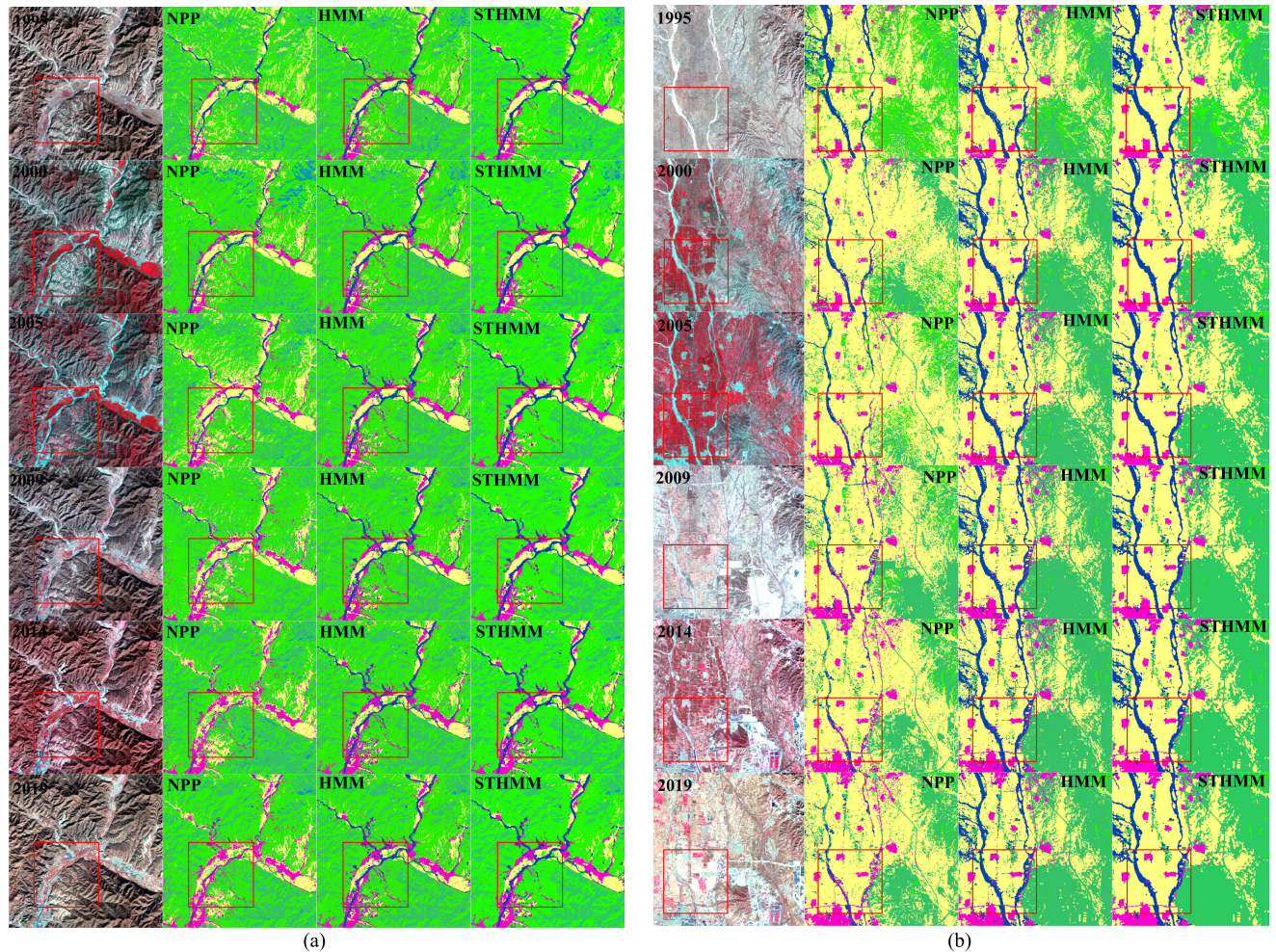
IEEE *Access*

C. Liu *et al.*: Spatial-Temporal Hidden Markov Model for Land Cover Classification Using Multitemporal Satellite Images

FIGURE 5. Local visualization comparison of postprocessing results from 1995 to 2019 (a) and (b): Landsat satellite images, NPP: no postprocessing classification results, HMM: classification results with HMM processing, STHMM: classification results of STHMM postprocessing.

a general standard for evaluating the classification of remote sensing images, mainly from a global perspective, to evaluate the accuracy of the classification results. The kappa coefficient represents the ratio of error reduction between classification and completely random classification, which can be used to evaluate the consistency and credibility of multiclassification results of remote sensing images. At the same time, the mean and standard deviation of the accuracy of all years are also listed. The mean reflects the accuracy of the classification results. The standard deviation reflects the stability of the classification results. In Table 1, it can be seen that the average overall accuracy of NPP is 0.89, the standard deviation is 0.39, and the original classifier has high classification accuracy and stability. The classification accuracy with HMM is significantly higher than that of NPP. The overall accuracy and Kappa coefficient are improved by 2.02 and 2.21, respectively. The HMM considers the multitemporal correlation between coverage types in different periods. The results of HMM processing can reflect more real features of ground change, but this method does not consider the spatial

relationship between different coverage types; that is, the similarity between coverage types with similar spatial distances is higher. The results of the spatial and temporal relationships show the best classification advantages compared to the other two methods. It has higher classification accuracy (OA = 92.76, Kappa = 92.74) and lower root mean square error (0.13). Overall, the STHMM shows the best classification accuracy.

2) TEMPORAL AND SPATIAL DISTRIBUTION EVALUATION

In fact, the accuracy of the classification results depends largely on the distribution of the samples and does not fully reflect the similarity between the real features and the classification results. Multitemporal land cover results often have a certain correlation in spatial-temporal distribution. For most feature types, the type of land cover changes with time is largely unchanged, and only a small number of feature types will change, as will the type of land cover changes in space. The closer the space is, the greater the similarity of the features. Therefore, a joint probability is used to judge the
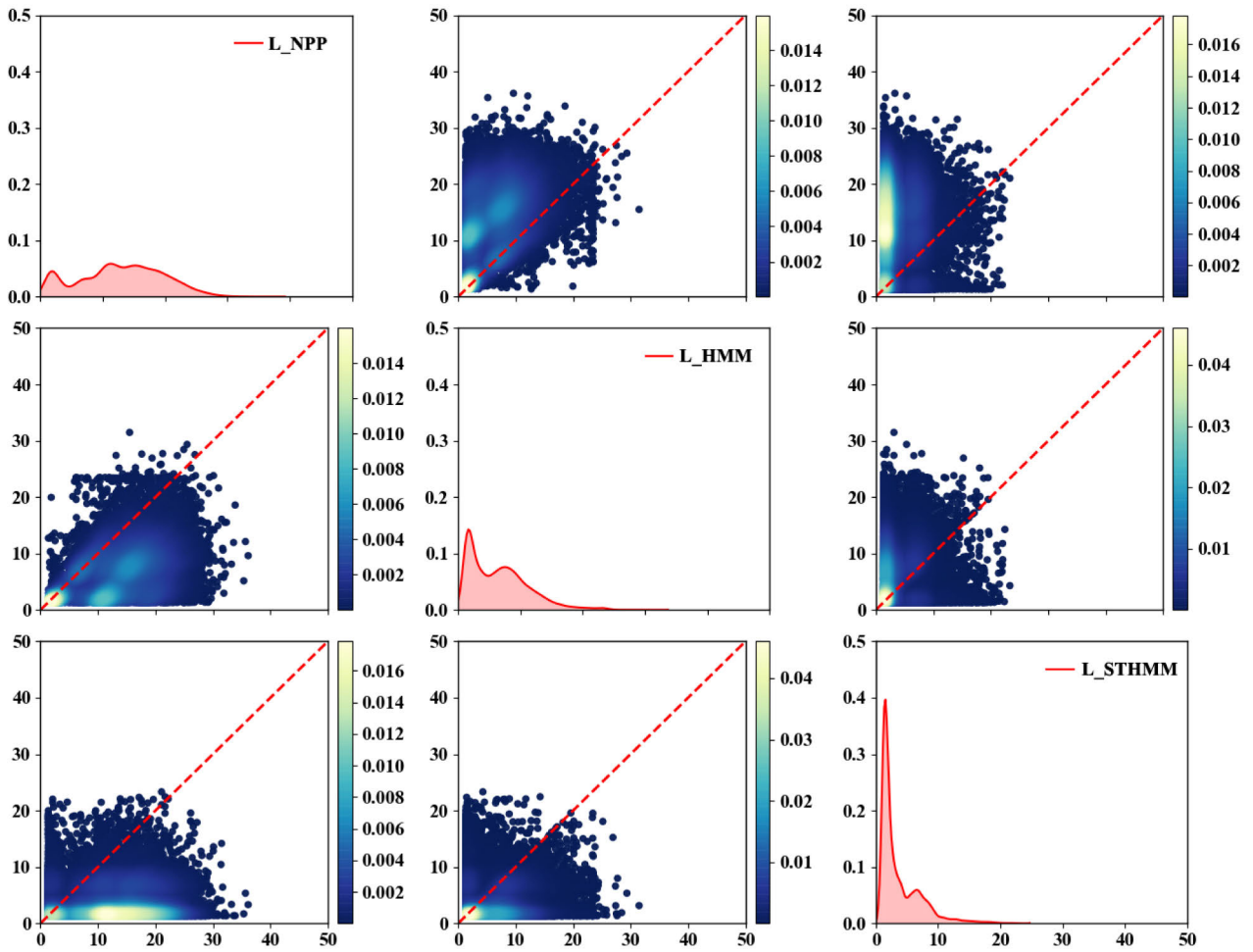
C. Liu *et al.*: Spatial-Temporal Hidden Markov Model for Land Cover Classification Using Multitemporal Satellite Images

IEEE *Access*

FIGURE 6. The distribution of indicators, the smaller the reliability of the results, the greater the spatial and temporal distribution of the decomposition results is in line with the actual situation, where the graphs on the diagonal represent the histogram distribution of the three indicators L_NPP, L_HMM, and L_STHMM. The graphs on the nondiagonal line are two-dimensional scatter plots with different classification indexes, and the colors in the graphs indicate the density of the scatter plots.

time series classification results, and the joint probability is calculated by the joint probability of classification results in each period, which reflects the continuity of pixels in space and time. The evaluation index is calculated by the following formula:

$$P = \prod_{t=1}^{T-1} P(i_t|O) P_s(i_t) P(i_{t+1}|i_t) \qquad (15)$$

To avoid the joint probability value being too small, the logarithm is taken as:

$$L(P) = -\sum_{t=1}^{T-1} (\log P(i_t|O) + \log P_s(i_t) + \log P(i_{t+1}|i_t)) \qquad (16)$$

where $P(i_{t+1}|i_t)$ is the transition probability of the state from time t to time t+1, $P(i_t|O)$ indicates the state i_t probability at time t, and $P_s(i_t)$ is the spatial probability at time t.

To more intuitively reflect the changes in the indicators of different methods, we compare any two results and draw the scatter matrix. The result is shown in Figure 6. It can be seen in the two-dimensional scatter plots constructed by L_NPP and L_HMM that the high-density points are closer to the L_HMM coordinate axis, indicating that the HMM index is generally higher than the NPP index value. The HMM considers the time relationship between images in different periods, and whether it is the time distribution of construction land or vegetation is more reasonable. It can be seen in the two-dimensional scatter plots constructed by L_STHMM and L_HMM that the high-density points are closer to the L_STHMM coordinate axis, while the distribution chart shows a lighter color, with 40% of the index value near 2. STHMM also considers that to understand the spatial-temporal relationship between different types, the L_STHMM indicator showed the lowest, indicating that the spatial-temporal distribution of its classification results is the most reliable.

IV. DISCUSSION

There are two key parameters in the spatial-temporal classification method proposed in this paper, which play a decisive
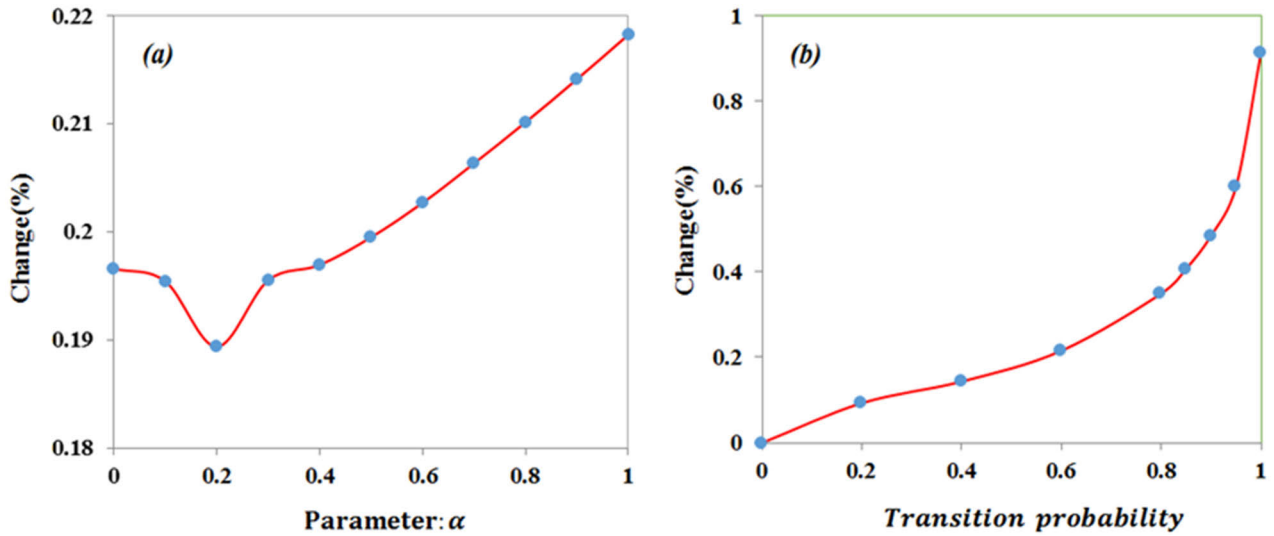
FIGURE 7. Sensitivity analysis of key parameters.

TABLE 1. Algorithm flow of spatial-temporal HMM classifier.

Algorithm1. Our proposed algorithm for Spatial-temporal HMM Classifier
Input: Training samples
Output: Multitemporal classification
Initialization: iterations IT, weight coefficient μ,
For t=1:T Classify pixel for each year $P(i_t|o_t)\leftarrow$Compute initial probability by SAE $P_s(i_t|o_t)\leftarrow$Optimizing initial probability by EWR End For it =1:IT $\quad\pi\leftarrow\frac{\sum_{t=1}^{T}P(i_t|o_t)}{T}$ Compute initial state probability $\quad$For t=1 to T do $\quad\quad P(o_t|i_t)\leftarrow$Compute observation probability by Bayes $\quad$End $\quad$For t=1 to T do $\quad\quad P_t(i_t|O)\leftarrow$Compute marginal probability by Forward-Backward algorithm $\quad$End $\quad$For t=1 to T-1 do $\quad\quad A_{tt+1}\leftarrow$HMM transition matrix by EM algorithm $\quad$End $\quad$For t=1 to T do $\quad\quad P_s(i_t|O)\leftarrow$Compute space-probability by EWR $\quad\quad P(i_t|O)\leftarrow(1-\alpha)P_s(i_t)+\alpha P_t(i_t|O)$ Update marginal probability $\quad$End End For t=1 to T do $\quad q_i\leftarrow\underset{q_i}{\text{argmax}}\,P(i_t|O,\lambda)$ $\quad\quad\quad$Assign optimal label End

role in the classification results of multiple temporal phases. Normally, the transformation probability between different types plays a crucial role in constructing multitemporal

remote sensing classification [34]–[37]. The conversion probability is determined by the regional environment and development. This paper refers to the design of the conversion probability in the literature. It is a set criterion, but it can only reflect the changing trend between images in different periods; it is an estimate, and it cannot truly represent the actual transformation probability. At the same time, the spatial-temporal weight parameters also affect the classification results of multitemporal remote sensing images; too high will lose the spatial correlation between pixels, and too low will also lose some local details. Therefore, this paper analyzes the changes in the two parameters to study the changes between different types of features in each period. In the case of a given weighting factor, the transformation probability varies from 0 to 1, and in the case of a given transformation probability, the weighting factor varies from 0 to 1.

Fig. 7(a) represents the change rate curve of remote sensing image classification in different periods under the given transformation probability of 0.5. It can be seen in the figure that as the weighting factor increases, the spatial correlation between the pixels gradually weakens, and the rate of change between different feature types shows a trend of decreasing first and then increasing, indicating that as the weighting factor increases, the correlation of the distribution characteristics of features in time increases first and then decreases. Therefore, the appropriate weighting factor is. It is very important to determine the classification accuracy of the image to a certain extent. In the case of 8(b) in the figure, when the weighting factor is set to 0.5, as the transformation probability continues to increase, the rate of change of features in different periods shows an increasing trend, Usually, within a short period of time, closer to 90% of the feature types will not change in a similar time. Therefore, this paper believes that without any prior knowledge, it is relatively reasonable to set the transformation probability to 0.9. The smaller the weighting

C. Liu *et al.*: Spatial-Temporal Hidden Markov Model for Land Cover Classification Using Multitemporal Satellite Images

IEEE*Access*

TABLE 2. NPP, HMM and STHMM classification accuracy tests for each period from 1995 to 2019.

Year	OA			Kappa		
	NPP	HMM	STHMM	NPP	HMM	STHMM
1995	89.42	91.66	**92.97**	89.41	91.64	**92.95**
2000	89.50	91.60	**92.73**	89.48	91.58	**92.71**
2005	89.01	91.90	**92.78**	88.99	91.88	**92.76**
2009	89.32	91.29	**92.77**	89.30	91.27	**92.75**
2010	89.28	91.12	**92.54**	89.26	91.11	**92.52**
2019	90.16	91.46	**92.79**	90.14	91.44	**92.77**
Mean ± Std	89.45±0.39	91.65±0.28	**92.76±0.13**	89.43±0.39	91.64±0.28	**92.74±0.13**

factor is, the more spatial correlation will be considered, and it will be appropriate. To improve the classification accuracy of multitemporal images, it can be set in the range of 0.1-0.3.

V. CONCLUSION

Time-series vegetation classification products are of great significance in the study of regional and global changes. Satellite remote sensing images are the main means to quickly obtain large-scale time-series land cover products. This article discusses and studies the key issues in the development of time-series remote sensing vegetation classification using satellite remote sensing images. The main research conclusions are as follows:

(1) The forward-backward algorithm is used to solve the optimal classification label sequence under the condition of HMM parameter determination, and the spatial correlation between the classification labels is statistically considered. This paper proposes a spatial-temporal hidden Markov for multitemporal classification. In terms of evaluation indicators, this paper also proposes a new comprehensive evaluation index for multitemporal remote sensing classification. It evaluates the classification results from actual measurement points, spatial and temporal distributions, and changes. The results show that the hidden Markov model considering the spatial-temporal relationship proposed in this paper performs best in spatial-temporal continuity and accuracy.

(2) This paper conducts a sensitivity analysis of the spatial weighting factor and transformation probability. The results show that a smaller spatial weighting factor helps to improve the stability of the classification results in different periods. At the same time, in adjacent periods, the outside world is under natural development. Most of the features in different periods will not change, which is consistent with the current research results. In the future, we will mine more elaborate classification transformation laws or use more intelligent methods to obtain more objective results. Under a more elaborate category configuration, we will further verify the generality of the labeling and evaluation algorithms proposed in this paper.

REFERENCES

[1] G. B. Bonan, "Forests and climate change: Forcings, feedbacks, and the climate benefits of forests," *Science*, vol. 320, no. 5882, pp. 1444–1449, Jun. 2008.

[2] B. Basnet and A. Vodacek, "Tracking land use/land cover dynamics in cloud prone areas using moderate resolution satellite data: A case study in central africa," *Remote Sens.*, vol. 7, no. 6, pp. 6683–6709, May 2015.

[3] A. Descals, Z. Szantoi, E. Meijaard, H. Sutikno, G. Rindanata, and S. Wich, "Oil palm (Elaeis guineensis) mapping with details: Smallholder versus industrial plantations and their extent in riau, sumatra," *Remote Sens.*, vol. 11, no. 21, p. 2590, Nov. 2019.

[4] T. A. Schroeder, S. P. Healey, G. G. Moisen, T. S. Frescino, W. B. Cohen, C. Huang, R. E. Kennedy, and Z. Yang, "Improving estimates of forest disturbance by combining observations from landsat time series with U.S. forest service forest inventory and analysis data," *Remote Sens. Environ.*, vol. 154, pp. 61–73, Nov. 2014.

[5] A. H. W. Seydack, G. Durrheim, and J. H. Louw, "Spatiotemporally interactive growth dynamics in selected south african forests: Edaphoclimatic environment, crowding and climate effects," *Forest Ecol. Manage.*, vol. 261, no. 7, pp. 1152–1169, Apr. 2011.

[6] B. Li, F. Huang, L. Qin, H. Qi, and N. Sun, "Spatio-temporal variations of carbon use efficiency in natural terrestrial ecosystems and the relationship with climatic factors in the songnen plain, China," *Remote Sens.*, vol. 11, no. 21, p. 2513, Oct. 2019.

[7] Wu, Liu, Sun, Su, Wang, Yang, Liao, He, Li, Zhang, and Zhang, "Estimating rainfall interception of vegetation canopy from MODIS imageries in southern China," *Remote Sens.*, vol. 11, no. 21, p. 2468, Oct. 2019.

[8] M. A. Wulder, J. C. White, S. N. Goward, J. G. Masek, J. R. Irons, M. Herold, W. B. Cohen, T. R. Loveland, and C. E. Woodcock, "Landsat continuity: Issues and opportunities for land cover monitoring," *Remote Sens. Environ.*, vol. 112, no. 3, pp. 955–969, Mar. 2008.

[9] K. Karalas, G. Tsagkatakis, M. Zervakis, and P. Tsakalides, "Land classification using remotely sensed data: Going multilabel," *IEEE Trans. Geosci. Remote Sens.*, vol. 54, no. 6, pp. 3548–3563, Jun. 2016.

[10] P. Gong, "Finer resolution observation and monitoring of global land cover: First mapping results with Landsat TM and ETM+ data," *Int. J. Remote Sens.*, vol. 34, nos. 7–8, pp. 2607–2654, 2013.

[11] X. Liu, G. Hu, Y. Chen, X. Li, X. Xu, S. Li, F. Pei, and S. Wang, "High-resolution multi-temporal mapping of global urban land using landsat images based on the Google Earth engine platform," *Remote Sens. Environ.*, vol. 209, pp. 227–239, May 2018.

[12] D. Potere, A. Schneider, S. Angel, and D. L. Civco, "Mapping urban areas on a global scale: Which of the eight maps now available is more accurate?" *Int. J. Remote Sens.*, vol. 30, no. 24, pp. 6531–6558, Nov. 2009.

[13] R. Dong, C. Li, H. Fu, J. Wang, W. Li, Y. Yao, L. Gan, L. Yu, and P. Gong, "Improving 3-m resolution land cover mapping through efficient learning from an imperfect 10-m resolution map," *Remote Sens.*, vol. 12, no. 9, p. 1418, Apr. 2020.

[14] W. Wu, C. Zucca, F. Karam, and G. Liu, "Enhancing the performance of regional land cover mapping," *Int. J. Appl. Earth Observ. Geoinf.*, vol. 52, pp. 422–432, Oct. 2016.

[15] E. K. Melaas, M. A. Friedl, and Z. Zhu, "Detecting interannual variation in deciduous broadleaf forest phenology using landsat TM/ETM+ data," *Remote Sens. Environ.*, vol. 132, pp. 176–185, May 2013.

[16] C. Gómez, J. C. White, M. A. Wulder, and P. Alejandro, "Historical forest biomass dynamics modelled with landsat spectral trajectories," *ISPRS J. Photogramm. Remote Sens.*, vol. 93, pp. 14–28, Jul. 2014.

[17] M. Broich, M. C. Hansen, P. Potapov, B. Adusei, E. Lindquist, and S. V. Stehman, "Time-series analysis of multi-resolution optical imagery for quantifying forest cover loss in sumatra and kalimantan, indonesia," *Int. J. Appl. Earth Observ. Geoinf.*, vol. 13, no. 2, pp. 277–291, Apr. 2011.

[18] G. Azzari and D. B. Lobell, "Landsat-based classification in the cloud: An opportunity for a paradigm shift in land cover monitoring," *Remote Sens. Environ.*, vol. 202, pp. 64–74, Dec. 2017.

[19] D. Simonetti, E. Simonetti, Z. Szantoi, A. Lupi, and H. D. Eva, "First results from the phenology-based synthesis classifier using landsat 8 imagery," *IEEE Geosci. Remote Sens. Lett.*, vol. 12, no. 7, pp. 1496–1500, Jul. 2015.

[20] M. Padilla, S. V. Stehman, J. Litago, and E. Chuvieco, "Assessing the temporal stability of the accuracy of a time series of burned area products," *Remote Sens.*, vol. 6, pp. 2050–2068, Apr. 2014.

[21] D. Pouliot, "Development and assessment of a 250 m spatial resolution MODIS annual land cover time series (2000-2011) for the forest region of Canada derived from change-based updating," *Remote Sens. Environ.*, vol. 140, pp. 731–743, Oct. 2014.

[22] G. Xian, C. Homer, and J. Fry, "Updating the 2001 national land cover database land cover classification to 2006 by using landsat imagery change detection methods," *Remote Sens. Environ.*, vol. 113, no. 6, pp. 1133–1147, Jun. 2009.

[23] J. Gray and C. Song, "Consistent classification of image time series with automatic adaptive signature generalization," *Remote Sens. Environ.*, vol. 134, pp. 333–341, Jul. 2013.

[24] M. A. Friedl, D. Sulla-Menashe, B. Tan, A. Schneider, N. Ramankutty, A. Sibley, and X. Huang, "MODIS collection 5 global land cover: Algorithm refinements and characterization of new datasets," *Remote Sens. Environ.*, vol. 114, no. 1, pp. 168–182, Jan. 2010.

[25] F. Melgani and S. B. Serpico, "A Markov random field approach to spatio-temporal contextual image classification," *IEEE Trans. Geosci. Remote Sens.*, vol. 41, no. 11, pp. 2478–2487, Nov. 2003.

[26] S. Cai, D. Liu, D. Sulla-Menashe, and M. A. Friedl, "Enhancing MODIS land cover product with a spatial–temporal modeling algorithm," *Remote Sens. Environ.*, vol. 147, pp. 243–255, May 2014.

[27] J. Wang, Y. Zhao, C. Li, L. Yu, D. Liu, and P. Gong, "Mapping global land cover in 2001 and 2010 with spatial-temporal consistency at 250m resolution," *ISPRS J. Photogramm. Remote Sens.*, vol. 103, pp. 38–47, May 2015.

[28] T. Hoberg, F. Rottensteiner, R. Queiroz Feitosa, and C. Heipke, "Conditional random fields for multitemporal and multiscale classification of optical satellite imagery," *IEEE Trans. Geosci. Remote Sens.*, vol. 53, no. 2, pp. 659–673, Feb. 2015.

[29] S. P. Abercrombie and M. A. Friedl, "Improving the consistency of multitemporal land cover maps using a hidden Markov model," *IEEE Trans. Geosci. Remote Sens.*, vol. 54, no. 2, pp. 703–713, Feb. 2016.

[30] P. Duan, P. Ghamisi, X. Kang, B. Rasti, S. Li, and R. Gloaguen, "Fusion of dual spatial information for hyperspectral image classification," *IEEE Trans. Geosci. Remote Sens.*, early access, Nov. 11, 2020, doi: 10.1109/TGRS.2020.3031928.

[31] M. Lan, Y. Zhang, L. Zhang, and B. Du, "Global context based automatic road segmentation via dilated convolutional neural network," *Inf. Sci.*, vol. 535, pp. 156–171, Oct. 2020.

[32] L. Bruzzone, R. Cossu, and G. Vernazza, "Detection of land-cover transitions by combining multidate classifiers," *Pattern Recognit. Lett.*, vol. 25, no. 13, pp. 1491–1500, Oct. 2004.

[33] A. Banerjee, I. Dhillon, J. Ghosh, and S. Sra, "Generative model-based clustering of directional data," in *Proc. 9th ACM SIGKDD Int. Conf. Knowl. Discovery Data Mining*, 2003, pp. 19–28.

[34] F. Vuolo and C. Atzberger, "Improving land cover maps in areas of disagreement of existing products using NDVI time series of MODIS—Example for Europe," *Photogramm. Fernerkund. Geoinf.*, vol. 2014, no. 5, pp. 393–407, 2014.

[35] T. Kinoshita, K. Iwao, and Y. Yamagata, "Creation of a global land cover and a probability map through a new map integration method," *Int. J. Appl. Earth Observ. Geoinf.*, vol. 28, pp. 70–77, May 2014.

[36] W. Gong, S. Fang, G. Yang, and M. Ge, "Using a hidden Markov model for improving the spatial-temporal consistency of time series land cover classification," *ISPRS Int. J. Geo-Inf.*, vol. 6, no. 10, p. 292, Sep. 2017.

[37] A. Wehmann and D. Liu, "A spatial–temporal contextual Markovian kernel method for multi-temporal land cover mapping," *J. Photogramm. Remote Sens.*, vol. 107, pp. 77–89, Sep. 2015.

CHUNLIN LIU was born in Anhui, China, in 1989. He received the bachelor's degree from the Minzu University of China, in 2011, and the master's degree from the China University of Mining & Technology–Beijing, in 2014. He is currently pursuing the Ph.D. degree with the Minzu University of China.

WEI SONG received the Ph.D. degree from the School of Electronic and Information Engineering, Beijing Jiaotong University, in 2010.

He completed his postdoctoral research at Tsinghua University, in 2014, visited the Macau University of Science and Technology, in 2017, and visited the Scholar with the New Jersey Institute of Technology, from 2017 to 2018. Since 2014, he has been serving as a Leader for the School of Information Engineering, Minzu University of China.

CHUNXIA LU received the bachelor's degree in science from Northwest University, in 1987, the master's degree in physical geography from the Lanzhou Institute of Desert Research, Chinese Academy of Sciences, in 1998, and the Ph.D. degree in ecology from the Institute of Geographic Sciences and Natural Resources Research, Chinese Academy of Sciences, in 2001.

From 1987 to 1998, she worked with the Lanzhou Institute of Desert Research, Chinese Academy of Sciences. She has been working with the Institute of Geographic Sciences and Natural Resources Research, Chinese Academy of Sciences, since 2001.

JIANXIN XIA left the Postdoctoral Research Station of the School of Environmental Science and Engineering, Peking University, in 2002. Since 2002, he has been working with the School of Life and Environmental Sciences, Minzu University of China.

● ● ●